



## City Research Online

### City, University of London Institutional Repository

---

**Citation:** Liu, X. & Banerjee, J. R. (2015). An exact spectral-dynamic stiffness method for free flexural vibration analysis of orthotropic composite plate assemblies - Part II: Applications. *Composite Structures*, 132, pp. 1288-1302. doi: 10.1016/j.compstruct.2015.07.022

This is the accepted version of the paper.

This version of the publication may differ from the final published version.

---

**Permanent repository link:** <https://openaccess.city.ac.uk/id/eprint/12515/>

**Link to published version:** <https://doi.org/10.1016/j.compstruct.2015.07.022>

**Copyright:** City Research Online aims to make research outputs of City, University of London available to a wider audience. Copyright and Moral Rights remain with the author(s) and/or copyright holders. URLs from City Research Online may be freely distributed and linked to.

**Reuse:** Copies of full items can be used for personal research or study, educational, or not-for-profit purposes without prior permission or charge. Provided that the authors, title and full bibliographic details are credited, a hyperlink and/or URL is given for the original metadata page and the content is not changed in any way.

---

City Research Online:

<http://openaccess.city.ac.uk/>

[publications@city.ac.uk](mailto:publications@city.ac.uk)

---

# An exact spectral-dynamic stiffness method for free flexural vibration analysis of orthotropic composite plate assemblies - Part II: Applications

X. Liu\*, J.R. Banerjee

*School of Mathematics, Computer Sciences and Engineering, City University London,  
London EC1V 0HB, UK*

---

## Abstract

An exact spectral-dynamic stiffness method (S-DSM) for free vibration analysis of composite plates and plate assemblies has been proposed in Part I of this two-part paper. The main purpose of Part II paper is two-fold: (i) To validate and demonstrate the superiority of the proposed S-DSM and (ii) To establish exact benchmark solutions for free vibration of composite plate-like structures. The S-DSM is applied to a number of problems covering orthotropic composite plates and plate assemblies. It is demonstrated that the S-DSM gives exact solutions with high computational efficiency within low as well as high frequency ranges. The applications are completely general and the new development can handle complex plate shapes with any boundary conditions.

*Keywords:* Composite plate-like structures, spectral-dynamic stiffness method, free vibration analysis, enhanced Wittrick-Williams algorithm, arbitrary boundary conditions

---

## 1. Introduction

In Part I of this two-part paper [1], a novel method called the spectral-dynamic stiffness method (S-DSM) has been developed for exact free flexural vibration analysis of composite plate-like structures. The proposed method has no restrictions and is completely general to handle any boundary conditions covering any frequency range.

The intended aim of this Part II paper is to examine critically the elegance of the S-DSM presented in the Part I companion paper, particularly in terms of

---

\*Corresponding author

*Email address:* xiangliu06@gmail.com (X. Liu)

its efficiency, accuracy and versatility. Since S-DSM provides flexibility to consider general composite plate-like structures with different geometries and material properties when subjected to different boundary conditions, a vast quantity of results can be computed. However, the main aim of this paper, which is basically a result paper, is to illustrate the benefits of the S-DSM in free vibration analysis of composite plate-like structures. A selective and carefully chosen sample of examples are given in this paper for composite plates and plate assemblies. The results computed by using the S-DSM are compared and contrasted with finite element solutions and other published results wherever possible. All of the S-DSM results presented are accurate up to all figures given in order to serve as benchmarks. It should be kept in mind that even through the theory in Part I paper allows consideration of rotatory inertia, results in this Part II paper are computed without the rotatory inertia effects for the convenience of validation (with existing results) and benchmarking purposes.

For notational convenience, Part I of this two-part paper is referred to as Part I paper. The reference of sections and equations in the Part I paper will be denoted as Section I-(section number) and Eq. I-(equation number) respectively. For example, Eq. (1) in the Part I paper is written in short form as Eq. I-(1) in this Part II paper and so on.

This Part II paper is organised as follows. In Section 2, the convergence, computational efficiency and numerical stability of the proposed spectral dynamic stiffness method (S-DSM) is examined and results are demonstrated quite comprehensively. More specifically, Section 2.1 illustrates the enormously high computational efficiency and numerical accuracy of the S-DSM, whereas Section 2.2 discusses the numerical stability of the method covering low to high frequency ranges. In Section 3, the S-DSM is applied to composite plates with different boundary conditions including classical and non-classical elastic constraints. The S-DSM applications for different practical engineering plate-like structures are illustrated in Section 4. This Part II paper is completed with conclusions in Section 5.

## **2. Convergence, efficiency and numerical stability analysis**

As expected, the S-DSM gives highly accurate results very efficiently by using a relatively small number of terms in the series expansion. This is due to the completeness as well as the strong orthogonality of the series applied. The reason was explained in detail in Ref. [2] in the context of isotropic plates. It will be shown that considerable advantages of S-DSM still apply to composite plates and plate assemblies in the same way as isotropic plates. Additionally, the S-DSM is numerically stable for any number of terms in the series which makes it possible to achieve exact solutions. It is therefore, justified to call the current S-DSM an

exact method, and its results are, to all intents and purposes, exact solutions. All of the S-DSM results presented in this paper (except those for the convergence test in Table 1) are accurate up to all figures presented.

In the numerical implementation of S-DSM, the formulated infinite algebraic matrices of Eq. I-(29) had to be eventually truncated. Therefore, it is important to examine the convergence rate of the method. To this end, high convergence rate as well as high numerical efficiency of the S-DSM are confirmed by extensive convergence and computational efficiency tests. Also, it is shown that the exact and high efficiency features of S-DSM apply not only in the low frequency range but also in the medium to high frequency ranges.

### 2.1. Convergence and numerical efficiency

At first, the convergence and computational efficiency studies of the current S-DSM are performed for three representative cases of a square composite plate. The dimensions of the composite plate are:  $2a \times 2b$  where  $2a = 2b = 1m$  and the total plate thickness  $h = 1mm$ . The plate is composed of four graphite/epoxy laminae with the stacking sequence  $[0^\circ/90^\circ/90^\circ/0^\circ]$  and each ply has the same thickness  $h/4$ . The properties of the material are:  $E_1/E_2 = 10, G_{12}/E_2 = 0.5, \nu_{12} = 0.25, \rho = 1600kg/m^3$ . Three case studies with classical boundary conditions in the usual notion are FFFF, CCCC and CSCS. The four sequential letters denote respectively the boundary conditions along the right, up, left and down plate edges in an anticlockwise sense. The first eight nonzero natural frequencies are computed for these three cases by the current S-DSM using different numbers of terms  $M$  and  $N$  in the series with  $M = N$ . The results are shown in Table 1. The S-DSM results are compared with those of the finite element method (FEM) using a very fine mesh with  $300 \times 300$  S4R5 elements in ABAQUS. All of the results for both S-DSM and FEM were computed on a PC with a 3.40 GHz Intel 4-core processor and 8GB of memory. The numbers of significant digits (abbreviated as Sign. Dig.) and the total execution time for each case are tabulated in the last two columns of Table 1. In particular, the exact Levy solutions for the CSCS case agree with the current S-DSM results up to the last figure.

Clearly, the current S-DSM exhibits a very fast convergence rate with respect to the number of terms used in the series solution. With five terms included in the series, the first eight natural frequencies show 3 to 5 significant digit accuracy. For the FFFF case the convergence rate is very fast: a ten-term series solution leads to four significant figure accuracy whereas a forty-terms series leads to six significant figure accuracy. For the CCCC and CSCS cases, the convergence rate is even faster - a five(ten)-term series gives as much as five(six) significant digit accuracy. This must be regarded as an extremely fast convergence rate. Extensive further tests for other cases suggest that the convergence rate of the S-DSM is surely much faster than all of the other existing methods. Note that in the remainder of

Table 1: Convergence and computational efficiency test for the dimensionless natural frequencies of a composite plate composed of symmetric  $[0^\circ/90^\circ/90^\circ/0^\circ]$  graphite-epoxy laminates ( $E_1/E_2 = 10, G_{12}/E_2 = 0.5, \nu_{12} = 0.25, \rho = 1600 \text{ kg/m}^3$ ). The results computed by the current S-DSM with three different boundary conditions are compared with the FEM (ABAQUS) results using a fine mesh size  $300 \times 300$ .

$M = N$	$\lambda = 4\omega a^2 \sqrt{\rho h/D_{11}}$								Sign. Dig.	Exec. Time (s)
FFFF	4	5	6	7	8	9	10	11		
2	5.52289	10.9293	15.7047	22.3667	24.9148	30.1888	33.8370	34.4469	2	0.10
5	5.51308	<b>10.9292</b>	15.6436	<b>22.3665</b>	24.8992	30.1882	33.6491	34.4027	3	0.15
10	5.51224	<b>10.9292</b>	15.6404	<b>22.3665</b>	24.8980	<b>30.1881</b>	33.6378	34.3995	4	0.16
40	<b>5.51209</b>	<b>10.9292</b>	<b>15.6399</b>	<b>22.3665</b>	<b>24.8978</b>	<b>30.1881</b>	<b>33.6360</b>	<b>34.3990</b>	6	0.27
50	<b>5.51209</b>	<b>10.9292</b>	<b>15.6399</b>	<b>22.3665</b>	<b>24.8978</b>	<b>30.1881</b>	<b>33.6360</b>	<b>34.3990</b>	>6	0.32
FEM	5.5116	10.930	15.639	22.367	24.897	30.190	33.633	34.399	4	49.0
CCCC	1	2	3	4	5	6	7	8		
2	25.7355	39.5993	63.8418	65.0195	72.7797	87.4600	102.075	109.611	2	0.09
5	<b>25.7362</b>	<b>39.6015</b>	<b>63.8582</b>	<b>65.8489</b>	72.8058	92.5701	<b>103.158</b>	<b>122.731</b>	5	0.12
10	<b>25.7362</b>	<b>39.6015</b>	<b>63.8582</b>	<b>65.8489</b>	<b>72.8059</b>	<b>92.5702</b>	<b>103.158</b>	<b>122.731</b>	6	0.14
20	<b>25.7362</b>	<b>39.6015</b>	<b>63.8582</b>	<b>65.8489</b>	<b>72.8059</b>	<b>92.5702</b>	<b>103.158</b>	<b>122.731</b>	>6	0.16
FEM	25.736	39.602	63.856	65.854	72.805	92.571	103.17	122.73	4	43.0
CSCS	1	2	3	4	5	6	7	8		
2	23.6077	31.7388	51.4186	62.8144	68.3365	79.4211	83.1656	106.049	2	0.18
5	<b>23.6191</b>	31.7646	51.8833	62.8821	68.4472	82.6627	83.6884	108.602	5	0.36
10	<b>23.6191</b>	<b>31.7647</b>	<b>51.8835</b>	<b>62.8822</b>	<b>68.4476</b>	<b>82.6643</b>	<b>83.6887</b>	<b>108.605</b>	6	0.50
20	<b>23.6191</b>	<b>31.7647</b>	<b>51.8835</b>	<b>62.8822</b>	<b>68.4476</b>	<b>82.6643</b>	<b>83.6887</b>	<b>108.605</b>	>6	1.14
FEM	23.618	31.764	51.884	62.882	68.442	82.662	83.701	108.60	4	42.0
Levy(Exact)	23.6191	31.7647	51.8835	62.8822	68.4476	82.6643	83.6887	108.605	6	-

this paper, all S-DSM results are shown in bold which converge to the last rounded figure presented.

Table 1 also demonstrates that the current S-DSM is computationally efficient with as much as 100-fold advantage over the conventional FEM. To achieve results with four significant-figure accuracy for the first eight elastic natural frequencies, the FEM using ABAQUS required 42 to 49 seconds whereas the S-DSM took only 0.12 to 0.36 seconds. That is to say, with less than 1% of computation time for the FEM package ABAQUS, the results from S-DSM are more accurate.

In spite of the very fast convergence rate of the current S-DSM, one should also bear in mind that the boundedness of the results is similar to those of isotropic plates [2]. Convergence tests suggest that the results of the present S-DSM converge from below if the truncated-series building blocks have flexible boundary conditions than the original boundary condition, such as the CCCC case in Table 1. For the CCCC case, along the clamped edge  $x = a$ , for example, the original clamped boundary conditions in Eq. I-(21) are  $W(a, y) = 0$  and  $\phi_x(a, y) = 0$ , which can be exactly satisfied if  $M = N = \infty$ . However, in numerical implementation, the infinite series would have to be truncated at some stage with higher order terms omitted. Therefore, the building blocks of the truncated system of boundary condition are more flexible than the original clamped boundary

condition, which gives lower bound solutions for the natural frequencies. On the contrary, the DSM results converge from above if its building blocks for the boundary conditions are stiffer than the original boundary condition, such as for the FFFF case in Table 1. However, the boundedness can not be predicted if the building blocks contain both stiffer and more flexible boundary conditions for the modelled plate, such as a mixed case like CFFF. In any case, the boundedness properties mentioned above are not of any major consequence due to the highly accurate results presented (accurate up to all figures presented).

## 2.2. Analysis within medium to high frequency ranges and some observations on numerical stability

The fast convergence rate and numerical efficiency of the current S-DSM already shown (within low frequency range) in the last section are also robust and stable within the medium to high frequency ranges. This is a tremendous advantage which applies to individual composite plates as well as complex composite plate assemblies.

Table 2 shows the results for four different cases of a square isotropic plate covering low to high frequency ranges (from the 1st to the 1000th flexural natural modes). The first three cases are for a plate with different boundary conditions (FFFF, CCCC and CSCS) whereas the fourth case is for a CSCC plate with internal line support located at three-tenth of the edge ( $x/(2a) = 0.3$ ). The results for the isotropic plates were obtained by letting the orthotropic ratios of the plate materials to be 1. When using the current S-DSM, the first three cases are modelled by one S-DS plate element whereas the fourth case is modelled by two S-DS plate elements. All S-DSM results are presented with accuracy up to six significant figures. The number of terms used in the series expansion ( $M$  and  $N$ ) are indicated in the table. Also, the total computation time taken by the S-DSM for each case is recorded in the last column of Table 2. The results computed by the current method are compared with those obtained by other methods including the discrete singular convolution (DSC) method [3, 4], exact Levy solution [3] and Trigonometric Ritz method [5].

It is evident from Table 2 that the S-DSM behaves extraordinarily well in terms of accuracy and computational efficiency not only for the low frequency range, but also for the medium to high frequency ranges. With no more than 30 terms taken in the series solution, all of the 20 flexural natural frequencies covering low to high frequency ranges have six significant digit accuracy for all of the four cases. It can be seen that all S-DSM results for the CSCS case coincide with exact Levy solutions [3] as expected. Furthermore, those 20 highly accurate results for each case were obtained within 12 seconds in total. In particular, each of the FFFF and CCCC cases took less than 0.4 second which is indeed, a remarkable computational efficiency. This is to be expected since the current method takes

Table 2: Numerical stability study of the S-DSM. The results are presented for the frequency parameter  $\lambda = 4\omega a^2/\pi^2\sqrt{\rho h/D}$  using S-DSM for four cases from low (1-10th modes), and medium (20-100th modes) to high (200-1000th modes) frequencies. The first three cases are for isotropic square plates with different boundary conditions whereas the final case is for a CSCC square isotropic plate with internal line support located at three-tenth ( $x/(2a) = 0.3$ ) of the edge.

Mode Methods $M, N$	FFFF	CCCC		CSCS			CSCC with internal line support		
	S-DSM 25+25	S-DSM 25+25	DSC <sup>a</sup> 101×101	S-DSM 30+30	Levy <sup>b</sup> Exact	DSC <sup>a</sup> 101×101	S-DSM 2(25+25)	DSC <sup>c</sup> 101×101	Ritz(trig.) <sup>d</sup> 50×50
1	<b>0.00000</b>	<b>3.64606</b>	3.6461	<b>2.93333</b>	2.9333	2.9333	<b>4.90797</b>	4.9080	4.9080
2	<b>0.00000</b>	<b>7.43635</b>	7.4364	<b>5.54663</b>	5.5466	5.5466	<b>7.89990</b>	7.8999	7.9000
3	<b>0.00000</b>	<b>7.43635</b>	7.4364	<b>7.02430</b>	7.0243	7.0243	<b>12.1929</b>	12.1929	12.1932
4	<b>1.36461</b>	<b>10.9646</b>	10.9647	<b>9.58349</b>	9.5835	9.5835	<b>13.1294</b>	13.1295	13.1297
5	<b>1.98550</b>	<b>13.3319</b>	13.3320	<b>10.3567</b>	10.3567	10.3567	<b>15.1607</b>	15.1608	15.1612
6	<b>2.45909</b>	<b>13.3951</b>	13.3952	<b>13.0801</b>	13.0801	13.0802	<b>20.2351</b>	20.2353	20.2360
7	<b>3.52607</b>	<b>16.7180</b>	16.7182	<b>14.2057</b>	14.2057	14.2057	<b>20.4862</b>	20.4863	20.4870
8	<b>3.52607</b>	<b>16.7180</b>	16.7182	<b>15.6821</b>	15.6821	15.6821	<b>20.5496</b>	20.5498	20.5509
9	<b>6.19004</b>	<b>21.3303</b>	21.3305	<b>17.2597</b>	17.2597	17.2597	<b>23.2337</b>	23.2340	23.2356
10	<b>6.19004</b>	<b>21.3303</b>	21.3305	<b>20.2450</b>	20.2450	20.2451	<b>25.8856</b>	25.8860	25.8879
20	<b>15.4864</b>	<b>37.6251</b>	37.6257	<b>34.9090</b>	34.9090	34.9093	<b>41.3478</b>	41.3481	41.3507
40	<b>36.8797</b>	<b>68.6660</b>	68.6682	<b>64.5845</b>	64.5845	64.5857	<b>72.8807</b>	72.8826	72.8925
60	<b>56.8884</b>	<b>94.3824</b>	94.3854	<b>91.1837</b>	91.1837	91.1863	<b>105.022</b>	105.027	105.050
80	<b>81.1448</b>	<b>126.705</b>	126.712	<b>118.971</b>	118.971	118.975	<b>134.086</b>	134.092	134.120
100	<b>106.007</b>	<b>156.649</b>	156.660	<b>147.991</b>	147.991	147.993	<b>160.517</b>	160.530	160.586
200	<b>219.427</b>	<b>290.220</b>	290.254	<b>281.655</b>	281.655	281.668	<b>306.030</b>	306.046	306.182
400	<b>462.626</b>	<b>561.364</b>	561.465	<b>550.555</b>	550.555	550.576	<b>580.000</b>	580.096	580.640
600	<b>704.645</b>	<b>826.952</b>	827.253	<b>814.177</b>	814.177	814.316	<b>846.353</b>	846.713	848.265
800	<b>951.601</b>	<b>1092.55</b>	1092.95	<b>1074.18</b>	1074.18	1074.41	<b>1113.88</b>	1114.19	1116.31
1000	<b>1197.00</b>	<b>1349.29</b>	1349.98	<b>1333.87</b>	1333.87	1334.31	<b>1380.36</b>	1381.06	1384.32
Sign. Dig.	<b>6</b>	<b>6</b>	4	<b>6</b>	6	4	<b>6</b>	4	3
Matrix size	<b>50</b>	<b>50</b>	10201	<b>120</b>	–	10201	<b>150</b>	10201	2500
Time(s)	<b>0.37</b>	<b>0.35</b>	–	<b>6.07</b>	–	–	<b>12.0</b>	–	–

<sup>a</sup> Discrete Singular Convolution method [3]

<sup>b</sup> Levy solution (exact) [3]

<sup>c</sup> Discrete Singular Convolution method [4]

<sup>d</sup> Trigonometric Ritz method [5]

advantage of the symmetry of the boundary conditions for these two cases. Also, mode shapes can be easily computed following the procedure described in Section I-5.2 of the Part I paper. For illustrative purposes, Fig. 1 shows the 1000th flexural mode shapes of a square isotropic plate with completely free and fully clamped boundary conditions. Both mode shapes shown in Fig. 1 illustrate the beauty of the mathematical pattern of symmetry. The 1000th flexural mode pattern of the completely free plate has repetitive structure whereas that of the fully clamped plate is somehow distorted. These delicate patterns are predicted accurately by the S-DSM using  $50 \times 50$  DS matrices. (It should be noted that the natural modes in this paper are for free flexural vibration only. For inplane natural modes, the corresponding S-DSM formulation needs to be developed using the general methodology described in this paper.)

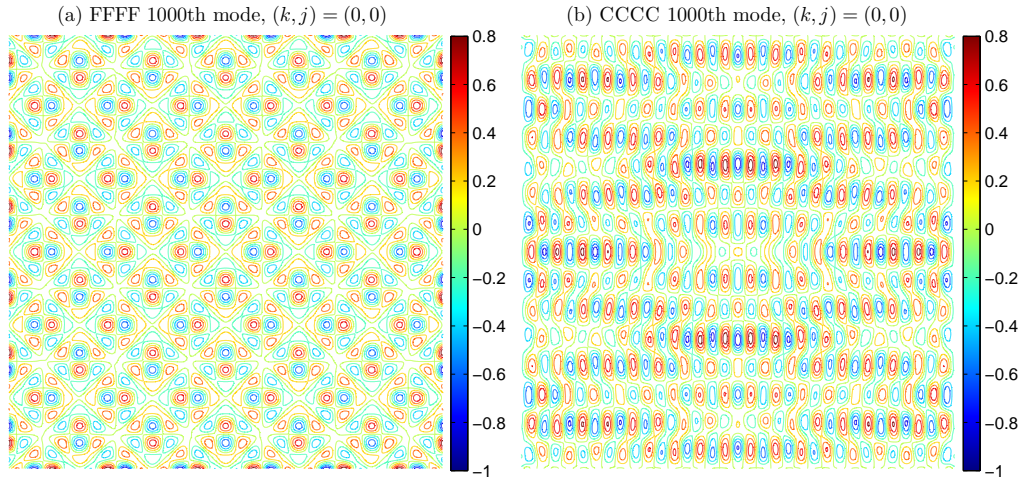


Figure 1: The 1000th flexural natural mode shapes of a square isotropic plate for (a) the completely free (FFFF) and (b) the fully clamped (CCCC) cases. Both modes are doubly symmetric in  $x$  and  $y$ :  $(k, j) = (0, 0)$ .

The current method is highly efficient mainly due to three reasons. (i) The first reason lies in the use of the series solution that satisfies the GDE exactly. The series solution establishes a complete solution space and is capable of represent the system accurately with minimum DOF. This was explained in detail in an earlier work [2] by the authors and hence is not repeated, (ii) The second reason is for the fact that the S-DSM is formulated on the *boundaries* in a *spectral* sense. There is an analogy between the current S-DSM and the boundary element and the spectral methods, in that the size of the DS matrix is significantly reduced. This has been mentioned in the last paragraph of Section I-3.2, (iii) Additionally, the efficiency gain can be attributed to the application of enhanced Wittrick-Williams (WW) algorithm for which the reason is briefly elucidated below.

The enhancement of WW algorithm presented in Part I paper has successfully resolved the so-called  $J_0$  problem for a fully clamped plate. This enhancement enabled the computation of high natural frequencies to any desired accuracy even using only a single plate element. The enhanced algorithm also takes full advantage of the one-to-one correspondence between  $J$ , the sign count related value of the formulated system, and the number of natural frequencies lying below a trial frequency. Consequently, it is very efficient to compute the exact solutions of any required natural frequency using a relatively small matrix. This is in sharp contrast to other methods. Rather than using the WW algorithm, most of other methods usually lead to either a determinant in the form  $\det(\mathbf{A}) = 0$  or a generalised eigenvalue problem in the form  $(\mathbf{K} - \omega^2\mathbf{M})\mathbf{x} = \mathbf{0}$ , both of which are solved by linear algebraic solvers. These methods are not so efficient especially

in the medium to high frequency ranges. This is because in order to solve the  $n$ th mode accurately, the size of the matrices  $\mathbf{K}$ ,  $\mathbf{M}$  or  $\mathbf{A}$  must be much bigger than  $n \times n$ . By contrast, the current S-DSM does not require a big matrix because of the application of the enhanced WW algorithm. Based on the results of Table 2, the comparison between the proposed S-DSM and other methods clearly shows the superiority of the S-DSM. For instance, in order to compute the first 1000 flexural natural modes, the discrete singular convolution method (DSC) [3, 4] needs to use a grid of  $101^2$  to define the domain points which leads to several matrices of size  $10201 \times 10201$ . The computed DSC results of all three cases are quite accurate for the first ten modes, but the results for higher than the 10th have accuracy of only four significant figures. The Trigonometric Ritz method [5] on the other hand, used  $M = N = 50$  series leading to  $2500 \times 2500$  matrices, but it still gives results with only three significant-figure accuracy for the natural frequencies that are higher than the 60th mode. In comparison, the S-DSM with  $M = N = 30$  series solution leads to four  $50 \times 50$  DS matrices (for different symmetric/antisymmetric cases) giving over 1000 modes with accuracy of six significant figures. Use of  $M = N = 30$  in the series solution leads to a  $120 \times 120$  DS matrix for the CSCS case, which is capable of computing over 1000 modes with as many as six significant figures. In the fourth example, the plate is modelled as a two-plate assembly. Accordingly, the S-DSM uses a  $M = N = 25$  series solution for both plate elements, which finally led to a  $150 \times 150$  matrix and gave the first 1000 natural frequencies with at least six significant figures.

Furthermore, the current S-DSM is versatile to handle any arbitrary boundary conditions like free edges as easily as the simply support or clamped edges. The exact solutions in the first column of Table 2 seem to be by far, the very first set of exact results reported for free flexural vibration of a completely free plate covering from low to high frequency ranges. Some of the other methods may experience difficulties particularly in the medium to high frequency ranges. This is certainly true for the conventional FEM. Some other methods may encounter obstacles when treating free boundary conditions, such as the discrete singular convolution (DSC) method [3, 4]. To overcome the problem in DSC, an iteratively matched boundary scheme based on finite difference was proposed in the literature [6], but even then the results appear to be inaccurate even for low frequencies (for the FFFF case results, accuracy was only up to two to three significant figures for the first six natural frequencies [7]). The DSC results are likely to become progressively more inaccurate in the medium to high frequency ranges when free edge(s) is(are) considered in the analysis. Also, it is worth emphasising that for a completely free plate (FFFF), the first three natural frequencies are zero, corresponding to the three rigid body modes (one for transverse translation and two for rotation). These three zero natural frequencies can not be captured by most of the other analytical methods, but they can be captured by the current S-DSM aided

mainly through the application of the enhanced WW algorithm.

### 3. Individual composite plates with different boundary conditions

Having demonstrated its high accuracy, efficiency and numerical stability, the S-DSM is now applied for free vibration analysis of composite plates against the background that the subject has been covered extensively in the literature. It appears that almost all of the existing results for composite plates in the literature are not sufficiently accurate in general. To address this issue, four representative problems are investigated here to provide exact results as benchmark solutions. These are (i) a completely free composite plate (FFFF), (ii) a fully clamped composite plate (CCCC), (iii) a CSCC composite plate and (iv) two elastically supported composite plates (CFEE and EEEE). All S-DSM results are shown in bold and presented with at least six significant figures.

#### 3.1. Fully clamped orthotropic plates

Free vibration analysis of fully clamped orthotropic plates has received wide attentions in recent years by using different methods [8, 9, 10, 11, 12, 13]. In this section, plates with all edges clamped are analysed by using the S-DSM, see Table 3. The first eight dimensionless natural frequencies are presented for nine sets of parameters which comprise three different plate aspect ratios ( $b/a = 0.5, 1.0$  and  $2.0$ ) and three different orthotropy ratios ( $\Gamma$  and  $\Lambda$  were defined in Eq. I-(3) as  $(D_{12} + 2D_{66})/D_{11}$  and  $D_{22}/D_{11}$  respectively). The symmetric or antisymmetric properties of the mode shapes are denoted in Table 3 using the notation  $(k, j)$ , as defined in the Part I paper:  $k, j$  taking '0' and '1' to represent symmetric and antisymmetric modes respectively. For example, a (0,1) natural mode indicates that the mode shape is symmetric in  $x$  and antisymmetric in  $y$ . All S-DSM results in Table 3 have accuracy up to seven significant figures. The results are compared with the published ones as follows: Sakata and Takahashi [12] who used extended Kantorovich method, Sakata and Hosokawa [10] who employed an iterative method based on dual trigonometric series, and Xing and Liu [13] who utilised an analytical method based on separation of variables. In Table 3, most of the results of the iterative method by Sakata and Hosokawa [10] agree with the S-DSM results to the last presented figures. The results of Ref. [10] are the most accurate results other than the current S-DSM. (It should be noted that  $360 \times 360$  terms were used in the iterative method in Ref. [10], which was only applied to a fully clamped single plate.) The results obtained by Xing and Liu [13] on the other hand are lower than the present results and therefore serve as the lower bound solutions. This is because the solutions given by Xing and Liu [13] did not use a complete set of series as explained in an earlier paper by the present authors [2] (Ref. [14] also provided an explanation for this from another perspective).

Table 3: Dimensionless natural frequency parameters  $4\omega a^2 \sqrt{\rho h/D_{11}}$  for CCC orthotropic plates with different aspect ratios and orthotropy ratios. The results computed by the current S-DSM are compared with published results by other methods [10, 12, 13].

Mode	1	2	3	4	5	6	7	8
$\Gamma = 0.5, \Lambda = 1.0$								
$b/a = 0.5$	(0,0)	(1,0)	(0,0)	(1,0)	(0,1)	(1,1)	(0,1)	(0,0)
<b>S-DSM</b>	<b>95.38622</b>	<b>118.4909</b>	<b>165.5685</b>	<b>237.0667</b>	<b>251.9630</b>	<b>269.9789</b>	<b>305.6628</b>	<b>331.2510</b>
Ext. Kant. <sup>a</sup>	95.391	118.502	165.583	–	251.965	269.987	305.677	–
ASV <sup>b</sup>	94.725	117.182	164.294	–	251.755	269.323	304.619	–
$b/a = 1.0$	(0,0)	(0,1)	(1,0)	(1,1)	(0,0)	(0,0)	(0,1)	(1,0)
<b>S-DSM</b>	<b>33.91205</b>	<b>69.68298</b>	<b>69.68298</b>	<b>98.43219</b>	<b>127.3822</b>	<b>127.8356</b>	<b>151.2807</b>	<b>151.2807</b>
IM(DTS) <sup>c</sup>	33.91205	69.68298	69.68298	98.43219	127.3822	127.8356	–	–
Ext. Kant. <sup>a</sup>	33.917	69.687	69.687	98.440	127.613*	127.613*	151.290	151.290
ASV <sup>b</sup>	33.174	69.254	69.254	97.795	127.382*	127.382*	150.754	150.754
$b/a = 2.0$	(0,0)	(0,1)	(0,0)	(0,1)	(1,0)	(1,1)	(1,0)	(0,0)
<b>S-DSM</b>	<b>23.84656</b>	<b>29.62273</b>	<b>41.39213</b>	<b>59.26667</b>	<b>62.99076</b>	<b>67.49474</b>	<b>76.41570</b>	<b>82.81276</b>
IM(DTS) <sup>c</sup>	23.84656	29.62273	41.39213	59.26668	62.99076	–	–	–
Ext. Kant. <sup>a</sup>	23.681	29.625	41.396	–	62.991	67.497	76.419	–
ASV <sup>b</sup>	23.848	29.296	–	–	62.939	–	–	–
$\Gamma = 1, \Lambda = 0.5$								
$b/a = 0.5$	(0,0)	(1,0)	(0,0)	(0,1)	(1,1)	(1,0)	(0,1)	(0,0)
<b>S-DSM</b>	<b>75.20593</b>	<b>110.2557</b>	<b>167.0508</b>	<b>187.2631</b>	<b>224.3542</b>	<b>244.5813</b>	<b>283.2921</b>	<b>342.3434</b>
$b/a = 1.0$	(0,0)	(0,1)	(1,0)	(1,1)	(0,0)	(0,0)	(1,0)	(0,1)
<b>S-DSM</b>	<b>32.27132</b>	<b>58.99198</b>	<b>71.50391</b>	<b>98.81160</b>	<b>100.4166</b>	<b>130.7193</b>	<b>140.9902</b>	<b>155.9831</b>
$b/a = 2.0$	(0,0)	(0,1)	(0,0)	(0,1)	(1,0)	(1,0)	(1,1)	(1,0)
<b>S-DSM</b>	<b>24.22422</b>	<b>29.84760</b>	<b>39.30346</b>	<b>52.53977</b>	<b>63.80830</b>	<b>69.46948</b>	<b>70.10799</b>	<b>80.33487</b>
$\Gamma = 0.5, \Lambda = 0.5$								
$b/a = 0.5$	(0,0)	(1,0)	(0,0)	(0,1)	(1,1)	(1,0)	(0,1)	(1,1)
<b>S-DSM</b>	<b>71.36246</b>	<b>100.1084</b>	<b>152.8245</b>	<b>181.8111</b>	<b>206.0119</b>	<b>228.1808</b>	<b>250.8386</b>	<b>318.3802</b>
Ext. Kant. <sup>a</sup>	71.371	100.126	152.844	181.816	206.026	–	250.861	–
ASV <sup>b</sup>	70.524	98.828	151.822	181.529	205.209	–	249.726	–
$b/a = 1.0$	(0,0)	(0,1)	(1,0)	(1,1)	(0,0)	(1,0)	(0,0)	(0,1)
<b>S-DSM</b>	<b>29.97917</b>	<b>54.33666</b>	<b>67.79765</b>	<b>88.15909</b>	<b>94.73135</b>	<b>124.7665</b>	<b>126.5222</b>	<b>144.6635</b>
IM(DTS) <sup>c</sup>	29.97917	54.33666	67.79766	88.15910	94.73136	–	–	–
Ext. Kant. <sup>a</sup>	29.986	54.344	67.802	88.169	94.739	124.779	126.525	144.689
ASV <sup>b</sup>	29.329	53.831	67.509	87.591	–	–	126.377	144.279
$b/a = 2.0$	(0,0)	(0,1)	(0,0)	(0,1)	(1,0)	(0,0)	(1,1)	(1,0)
<b>S-DSM</b>	<b>23.50317</b>	<b>27.52424</b>	<b>35.43643</b>	<b>47.57875</b>	<b>62.83941</b>	<b>63.81277</b>	<b>66.54961</b>	<b>73.30698</b>
IM(DTS) <sup>c</sup>	23.50317	27.52425	35.43644	47.57876	62.83942	–	–	–
Ext. Kant. <sup>a</sup>	23.504	27.527	35.441	–	62.840	–	66.552	73.311
ASV <sup>b</sup>	23.399	27.258	–	–	62.806	–	66.436	–

<sup>a</sup> Extended Kantorovich [12]

<sup>b</sup> Analytical method based on Separation of Variables [13]

<sup>c</sup> Iterative Method (Dual Trigonometric Series) [10]

Therefore, the analytical method based on separation of variables given by Xing and Liu [13] is not really an ‘exact’ method.

It is found that ‘degenerate mode’ of clamped square plates does not only occur for square isotropic plates, but also emerges for square orthotropic plates as well, provided  $D_{22} = D_{11}$ , i.e. when  $\Lambda = 1, b/a = 1$ . The shapes of the degenerate modes have non-parallel nodal lines relative to the  $x$  and  $y$  axes. These degen-

erate modes can be calculated accurately by the current method and by the iterative method of Ref. [10], but can not be captured by the extended Kantorovich method [12] nor can it be captured by the analytical method based on separation of variables [13]. For instance, for the case  $\Gamma = 0.5$ ,  $\Lambda = 1$ ,  $b/a = 1$ , there should be two different doubly symmetric mode shapes  $(0, 0)$  for the sixth and seventh modes, but the extended Kantorovich method [12] and the analytical method based on separation of variables [13] gave only one repeated frequency (denoted by ‘\*’ in Table 3). As mentioned earlier, the inaccuracy of the two methods [12] and [13] can be attributed to the incompleteness of the series adopted in the analysis.

### 3.2. Completely free orthotropic plates

The next example is a plate whose edges are completely free (FFFF). This is the case for which a number of existing methods do not seem to work very well [7, 12, 15]. For example, the Rayleigh-Ritz method is poorly behaved for the FFFF case compared to other cases. This was pointed out by Leissa [15]. The Kantorovich method is not suitable either [12] for the FFFF case. As mentioned earlier, the discrete singular convolution method [7] also encounters difficulties when free boundary condition(s) is(are) involved. The inadequacies of these methods seems to be due to the difficulties in getting the solution satisfying accurately both the governing differential equation and the free boundary conditions.

In Table 4, the first eight nonzero dimensionless frequencies  $\omega a^2 \sqrt{\rho h / D_{11}}$  are computed for a completely free (FFFF) plate by using the present S-DSM. The results are compared with those obtained from Gorman’s superposition method [16] (GSM). The symmetric/antisymmetric properties of the corresponding mode shapes are denoted in parentheses  $(k, j)$ , just like the previous CCCC case. The first three natural frequencies for a completely free composite plate are zero as mentioned earlier due to rigid-body motion. All of the S-DSM results in Table 4 have accuracy up to six significant figures. These were computed with 25 terms adopted in the series expansion. In comparison, Gorman’s results [16] have only four significant-figure accuracy by using 15 terms in the series solution. As can be seen, Gorman’s results match the first four figures of the S-DSM results. Clearly, the S-DSM results presented here are more accurate than those in Ref. [16] and therefore, provide benchmark solutions for future comparison.

### 3.3. CSCC orthotropic plates

A further illustrative example is now considered when the plate is clamped on three edges whilst simply supported on the other (CSCC). The first eight dimensionless natural frequencies are computed by the present S-DSM, which are then compared with those obtained by the extended Kantorovich method reported by Sakata *et al.* [12] and also by the analytical method based on separation of variables given by Xing and Liu [13]. These are shown in Table 5. With  $M = N = 10$

Table 4: Dimensionless natural frequency parameters  $\omega a^2 \sqrt{\rho h / D_{11}}$  for completely free (FFFF) orthotropic plates ( $\sqrt{\nu_{12}\nu_{21}} = 0.333$ ) with three different aspect ratios and three orthotropy ratios. The results computed by the current S-DSM are compared with the published results by Gorman's superposition method (GSM) [16].

Mode	4	5	6	7	8	9	10	11
$\Gamma = 0.5, \Lambda = 1.0$								
$b/a = 0.5$	(1,1)	(0,0)	(0,0)	(0,1)	(1,0)	(0,0)	(1,1)	(0,1)
<b>S-DSM</b>	<b>3.35576</b>	<b>5.28609</b>	<b>8.72091</b>	<b>14.5318</b>	<b>18.0250</b>	<b>21.7341</b>	<b>23.0981</b>	<b>26.4812</b>
$b/a = 1.0$	(1,1)	(0,0)	(0,0)	(0,1)	(1,0)	(0,0)	(1,1)	(0,1)
<b>S-DSM</b>	<b>1.69730</b>	<b>4.79982</b>	<b>6.04751</b>	<b>6.35770</b>	<b>6.35770</b>	<b>10.7427</b>	<b>14.6523</b>	<b>15.0676</b>
GSM	1.697	4.800	6.048	6.358	6.358	10.74	14.65	15.07
$b/a = 2.0$	(1,1)	(0,0)	(1,0)	(0,1)	(1,1)	(0,0)	(0,1)	(0,0)
<b>S-DSM</b>	<b>0.838939</b>	<b>1.32152</b>	<b>2.18022</b>	<b>3.63294</b>	<b>4.50625</b>	<b>5.43351</b>	<b>5.77452</b>	<b>6.62031</b>
GSM	0.8390	1.322	2.180	3.633	4.507	5.434	5.775	6.621
$\Gamma = 1, \Lambda = 0.5$								
$b/a = 0.5$	(0,0)	(1,1)	(1,0)	(0,1)	(0,0)	(1,0)	(1,1)	(0,0)
<b>S-DSM</b>	<b>5.31361</b>	<b>6.89510</b>	<b>14.8355</b>	<b>15.0112</b>	<b>15.6121</b>	<b>21.1778</b>	<b>25.8420</b>	<b>29.5634</b>
$b/a = 1.0$	(1,1)	(0,0)	(0,0)	(1,0)	(0,1)	(0,1)	(1,1)	(1,0)
<b>S-DSM</b>	<b>3.46670</b>	<b>3.68637</b>	<b>5.64068</b>	<b>7.99221</b>	<b>8.74231</b>	<b>10.9014</b>	<b>14.8570</b>	<b>15.2385</b>
GSM	3.467	3.686	5.641	7.992	–	–	14.86	15.24
$b/a = 2.0$	(0,0)	(1,1)	(0,1)	(1,0)	(0,0)	(0,0)	(1,1)	(0,1)
<b>S-DSM</b>	<b>0.940069</b>	<b>1.71073</b>	<b>2.62720</b>	<b>3.60196</b>	<b>5.05328</b>	<b>5.70380</b>	<b>5.87145</b>	<b>6.49600</b>
GSM	0.9401	1.711	–	3.602	5.053	5.704	5.872	–
$\Gamma = 0.5, \Lambda = 0.5$								
$b/a = 0.5$	(1,1)	(0,0)	(0,1)	(1,0)	(0,0)	(1,0)	(1,1)	(0,0)
<b>S-DSM</b>	<b>4.17236</b>	<b>5.29536</b>	<b>10.1021</b>	<b>14.3789</b>	<b>15.5634</b>	<b>18.2488</b>	<b>19.6372</b>	<b>23.9574</b>
$b/a = 1.0$	(1,1)	(0,0)	(0,0)	(1,0)	(0,1)	(0,1)	(0,0)	(1,1)
<b>S-DSM</b>	<b>2.10235</b>	<b>3.67815</b>	<b>5.61853</b>	<b>5.72442</b>	<b>6.81061</b>	<b>10.7826</b>	<b>11.1292</b>	<b>12.1991</b>
GSM	2.102	3.678	5.619	5.724	–	–	11.13	12.20
$b/a = 2.0$	(0,0)	(1,1)	(1,0)	(0,1)	(1,1)	(0,0)	(0,0)	(0,1)
<b>S-DSM</b>	<b>0.936535</b>	<b>1.02990</b>	<b>2.32114</b>	<b>2.59782</b>	<b>4.14046</b>	<b>4.98749</b>	<b>5.68129</b>	<b>5.86639</b>
GSM	0.9365	1.030	2.321	–	4.141	4.988	5.681	–

all S-DSM results have up to six significant-figure accuracy. From Table 5, it can be seen that most of the results from the Kantorovich method [12] agree up to four significant digits when compared with the S-DSM results. On the other hand, the results computed from the analytical method based on separation of variables [13] are slightly lower than those by the other two methods. The reason is similar to that for the fully clamped case, as explained earlier.

### 3.4. Plates with elastic constraints

In many practical applications, plate boundary motion is not necessarily completely restrained or free in terms of translation and/or rotation, but an intermediate situation on support condition can occur with nonzero generalised forces or displacements. This type of situation is particularly important because the boundary conditions may affect the modal behaviour significantly especially at low frequencies. Such type of boundary conditions can generally be modelled by elastic constraints, which require special treatments when applying methods like Ritz

Table 5: Dimensionless natural frequency parameters  $4\omega a^2 \sqrt{\rho h/D_{11}}$  are computed by the present S-DSM for CSCC rectangular orthotropic plates with three different aspect ratios and three orthotropy ratios. The results are compared with published results in Refs. [12] and [13].

$b/a$	Method	1	2	3	4	5	6	7	8
$\Gamma = 0.5, \Lambda = 1.0$									
0.5	<b>S-DSM</b>	<b>69.6830</b>	<b>98.4322</b>	<b>151.281</b>	<b>205.993</b>	<b>226.410</b>	<b>227.175</b>	<b>267.113</b>	<b>323.527</b>
	Ext. Kant. <sup>a</sup>	69.687	98.440	151.290	205.994	226.800	–	267.127	–
	ASV <sup>b</sup>	69.254	97.795	150.754	205.859	226.410	–	266.561	–
1	<b>S-DSM</b>	<b>29.6227</b>	<b>59.2667</b>	<b>67.4947</b>	<b>90.8335</b>	<b>111.707</b>	<b>126.268</b>	<b>137.568</b>	<b>145.986</b>
	Ext. Kant. <sup>a</sup>	29.625	59.270	67.497	90.838	111.711	126.268	137.574	145.990
	ASV <sup>b</sup>	29.296	59.021	67.331	90.528	–	126.178	–	145.751
2	<b>S-DSM</b>	<b>23.4466</b>	<b>28.0553</b>	<b>38.2735</b>	<b>54.6174</b>	<b>62.7933</b>	<b>66.6715</b>	<b>74.5307</b>	<b>76.7324</b>
	Ext. Kant. <sup>a</sup>	23.447	28.057	38.276	–	62.794	66.672	74.532	–
	ASV <sup>b</sup>	23.385	27.906	–	–	62.772	66.600	–	–
$\Gamma = 1, \Lambda = 0.5$									
0.5	<b>S-DSM</b>	<b>58.9920</b>	<b>98.8116</b>	<b>155.983</b>	<b>158.750</b>	<b>197.169</b>	<b>238.145</b>	<b>260.204</b>	<b>309.336</b>
1	<b>S-DSM</b>	<b>29.8476</b>	<b>52.5398</b>	<b>70.1080</b>	<b>90.0240</b>	<b>94.2645</b>	<b>129.744</b>	<b>132.730</b>	<b>141.846</b>
2	<b>S-DSM</b>	<b>23.9633</b>	<b>28.9005</b>	<b>37.4437</b>	<b>49.6932</b>	<b>63.6512</b>	<b>65.6301</b>	<b>69.5126</b>	<b>79.0936</b>
$\Gamma = 0.5, \Lambda = 0.5$									
0.5	<b>S-DSM</b>	<b>54.3367</b>	<b>88.1591</b>	<b>144.664</b>	<b>149.882</b>	<b>177.354</b>	<b>222.305</b>	<b>226.586</b>	<b>298.376</b>
	Ext. Kant. <sup>a</sup>	54.344	88.169	144.689	149.870	177.369	–	226.602	–
	ASV <sup>b</sup>	53.831	87.591	144.279	149.691	176.911	–	226.031	–
1	<b>S-DSM</b>	<b>27.5242</b>	<b>47.5788</b>	<b>66.5496</b>	<b>83.6343</b>	<b>83.9318</b>	<b>116.130</b>	<b>125.717</b>	<b>135.291</b>
	Ext. Kant. <sup>a</sup>	27.527	47.584	66.552	83.640	83.640	116.137	125.719	–
	ASV <sup>b</sup>	27.258	47.305	66.436	83.374	–	–	125.658	–
2	<b>S-DSM</b>	<b>23.2762</b>	<b>26.6183</b>	<b>33.5390</b>	<b>44.6057</b>	<b>59.7926</b>	<b>62.7162</b>	<b>66.0507</b>	<b>72.1837</b>
	Ext. Kant. <sup>a</sup>	23.277	26.620	33.542	–	–	62.716	66.052	72.185
	ASV <sup>b</sup>	23.235	26.501	–	–	–	62.702	66.000	–

<sup>a</sup> Extended Kantorovich [12]

<sup>b</sup> Analytical method based on Separation of Variables [13]

method (e.g., see [5]). For some other methods, elastic constraints are sometimes impossible to apply (e.g., see [10]). The elastic constraints can be represented easily when applying the current S-DSM. The procedure was described in Section I-4.2.

Table 6 includes two cases involving elastic boundary conditions, one for the CFEE isotropic plate and the other for the EEEE orthotropic plates. The Letter E is used to denote the elastic boundary conditions along the corresponding edges. The results are computed when both translational and rotational springs of magnitudes  $K(2a)^3/D_{11}$  and  $R(2a)/D_{11}$  respectively are attached to the corresponding edges of the composite plate. The first eight exact natural frequencies computed by the S-DSM are compared with those from two other methods, namely, the Trigonometric Ritz method [5], and the Fourier series based analytical method [17, 18]. The results based on the Trigonometric Ritz method [5] and the Fourier series based analytical method [17] appear to be very accurate for the first several (say, four) natural frequencies, but deteriorate for higher natural frequencies,

Table 6: The first eight dimensionless frequencies of isotropic and orthotropic plates with elastic boundary conditions. The parameters  $K(2a)^3/D_{11}$  and  $R(2a)/D_{11}$  are the dimensionless translational and rotational spring constants of elastic boundary supports, respectively. Ritz(trig.) represents Trigonometric Ritz method [5] and FSA is the Fourier series based analytical method [17].

Method	$\lambda = 4\omega a^2 \sqrt{\rho h / D_{11}}$								
	1	2	3	4	5	6	7	8	
Isotropic CFEE plate $a/b = 1$ ; $K(2a)^3/D_{11} = 10$									
$\frac{R(2a)}{D_{11}} = 1$	<b>S-DSM</b>	<b>7.53474</b>	<b>11.7090</b>	<b>24.3030</b>	<b>29.4441</b>	<b>33.0349</b>	<b>55.6938</b>	<b>63.4062</b>	<b>66.6260</b>
	Ritz(trig.)	7.535	11.709	24.304	29.445	33.037	55.697	–	–
	FSA	7.534	11.708	24.300	29.445	33.029	55.691	–	–
$\frac{R(2a)}{D_{11}} = 100$	<b>S-DSM</b>	<b>7.89965</b>	<b>12.5974</b>	<b>30.2210</b>	<b>34.5361</b>	<b>37.5783</b>	<b>61.0783</b>	<b>73.7551</b>	<b>77.5919</b>
	Ritz(trig.)	7.900	12.598	30.222	34.537	37.580	61.081	–	–
	FSA	7.899	12.597	30.218	34.537	37.574	61.077	–	–
Orthotropic EEEE plate, $D_{22}/D_{11} = 1/2$ , $D_{66} = D_{22}$ , $\nu_{12} = 0.3$ ; $K(2a)^3/D_{11} = 100$ , $R(2a)/D_{11} = 1000$									
$\frac{a}{b} = 1$	<b>S-DSM</b>	<b>16.6231</b>	<b>23.8935</b>	<b>25.1019</b>	<b>33.8718</b>	<b>37.5727</b>	<b>46.5825</b>	<b>51.9409</b>	<b>58.4520</b>
	Ritz(trig.)	16.623	23.894	25.102	33.871	37.572	46.582	–	–
$\frac{a}{b} = 2$	<b>S-DSM</b>	<b>22.9399</b>	<b>29.2019</b>	<b>41.8237</b>	<b>48.7375</b>	<b>55.3484</b>	<b>87.0557</b>	<b>93.1125</b>	<b>115.917</b>
	Ritz(trig.)	22.940	29.203	41.823	48.736	55.340	87.031	–	–

say, over the fifth mode. Clearly, the results computed by the S-DSM are much more accurate than those obtained by the two other methods for different values of elastic spring constants and plate aspect ratios.

#### 4. Complex engineering structures with practical applications

In the previous section, the current S-DSM was applied to four cases of individual composite plates. These cases are clearly for non-Levy type plates. Such analyses in an exact sense prior to this research were not possible earlier by using the conventional DSM. The current results have demonstrated the exactness, high efficiency of the S-DSM for any frequency range. In this section, the assembly procedure (another important advantage of the S-DSM) is illustrated by applying the method to three practical structures. Indeed, the current S-DSM can be effectively applied to any complex plate-like structures which can be modelled as an assembly of plates. Moreover, these structures can be subjected to any arbitrary boundary conditions. Unlike the previous DSM research, this development is not restricted to Levy-type plate assemblies. Note that because the problem of solving for the natural frequencies of a fully clamped plate (the so-called  $J_0$  problem) has been resolved, the current S-DSM is completely independent of the number of elements used in the analysis which is in a sharp contrast to most of the previous DSM developments for plate or shell assemblies especially within high frequency range. In the current method, minimum number of elements are used in the analysis unless there is a change in the geometry or material properties so as to reduce the computational cost.

The assembly procedure and the application of arbitrary boundary conditions for a complex structures were described in Section I-4. In what follows, three complex, but practical problems are analysed using the current S-DSM. In Section 4.1 below, a stepped cantilever laminated plate is investigated which may have application in aeronautical engineering. A three-span composite plate is then modelled in Section 4.2 which from a civil engineering point of view is significant. Finally, a class of irregularly shaped plates with different geometries and boundary conditions are considered in Section 4.3.

#### 4.1. A stepped cantilever laminated plate

This model can be used for preliminary dynamic analysis of composite aircraft wings [19, 20], fan blades of turbine or air conditioning system amongst others. Also, it can be used to determine the seismic response of some high-rise buildings [21]. The vibration of cantilever plate without step discontinuities in properties have been extensively covered, e.g., see [19, 22, 23, 24], but for a stepped cantilever plate, very few research papers have been published [21, 25]. In particular, Gorman and Singhal considered *isotropic* stepped cantilever plates using both superposition method and experiment [21]. On the other hand, Liu and Buchanan used finite element method to discuss moderately thick isotropic plates [25]. The difficulties arise not only from the specific boundary conditions, but also from the discontinuities of the properties in the connecting domains. An illustrative example is given where the current S-DSM can provide exact solutions for such structures made of composite material.

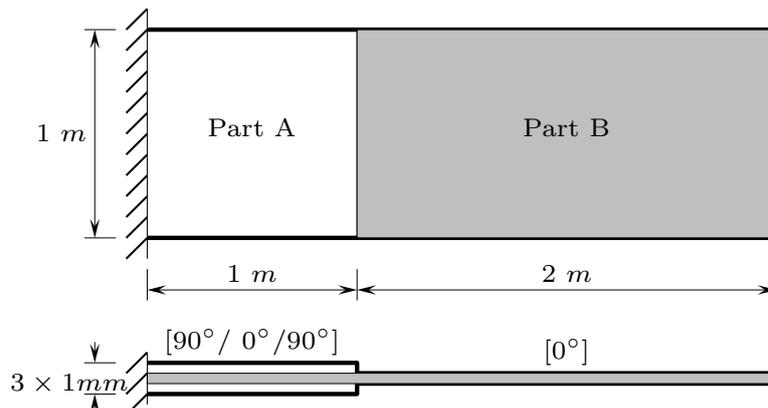


Figure 2: A stepped cantilever composite plate.

The stepped composite plate shown in Fig. 2 is cantilevered at the left hand end whereas the other edges are free. It is made of T-graphite/epoxy lamina with the material properties:  $E_1 = 185GPa$ ,  $E_2 = 10.5GPa$ ,  $G_{12} = 7.3GPa$ ,  $\nu_{12} = 0.28$ ,  $\rho = 1600kg/m^3$ . This plate consists of three laminae with the stacking

sequence  $[90^\circ/0^\circ/90^\circ]$ . Each ply is 1 mm thick. The top and bottom laminae extend at 1 m from the cantilever edge whereas the middle laminae is extended by a further 2 m as shown. It has not been possible to analyse this case by using previous versions of DSM.

Table 7: The first 20 natural frequencies for a cantilevered stepped plate as shown in Fig. 2. The results computed by the present S-DSM are compared with those obtained from FEM using ABAQUS.

Mode	S-DSM (Hz)	FEM (Hz)	Rel. Err. (%)	Mode	S-DSM (Hz)	FEM (Hz)	Rel. Err. (%)
1	<b>0.26805</b>	0.26805	0.00	11	<b>7.7125</b>	7.7126	0.00
2	<b>0.7179</b>	0.7178	-0.02	12	<b>9.4366</b>	9.4374	0.01
3	<b>1.2803</b>	1.2803	0.00	13	<b>9.5223</b>	9.5219	0.00
4	<b>2.5520</b>	2.5515	-0.02	14	<b>10.600</b>	10.601	0.01
5	<b>2.9367</b>	2.9368	0.00	15	<b>12.601</b>	12.602	0.00
6	<b>3.2194</b>	3.2195	0.00	16	<b>13.557</b>	13.558	0.00
7	<b>4.3369</b>	4.3364	-0.01	17	<b>14.449</b>	14.456	0.05
8	<b>5.1730</b>	5.1726	-0.01	18	<b>15.723</b>	15.727	0.03
9	<b>6.5466</b>	6.5472	0.01	19	<b>15.990</b>	15.992	0.01
10	<b>7.4840</b>	7.4856	0.02	20	<b>16.159</b>	16.164	0.03

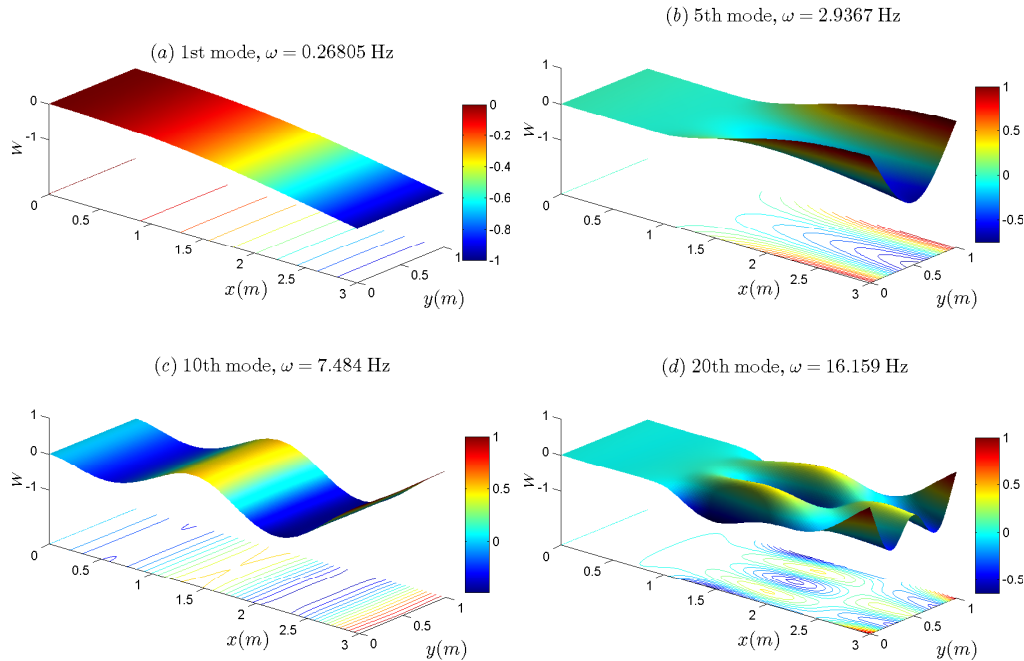


Figure 3: The 1st, 5th, 10th and 20th natural modes of the stepped cantilevered laminated plate as shown in Fig. 2.

The first 20 natural frequencies for the cantilever composite plate structure are obtained by using two method. These are the FE solutions using ABAQUS

and the present S-DSM, see Table 7. The very small differences in the results indicate excellent agreement between the methods. In the FE simulation,  $150 \times 150$  S4R5 elements were used for Part A, and  $200 \times 150$  elements for Part B of the composite plate shown in Fig. 2. The FE solutions are accurate up to four significant figures. On the other hand, when applying the current S-DSM to the same problem, the structure is idealised into two spectral-dynamic stiffness plate elements, namely, Part A and Part B. Part A is composed of three laminae with the lay-up  $[90^\circ/0^\circ/90^\circ]$  whereas Part B has only one lamina with ply angle  $0^\circ$ . The current S-DSM gives results with at least five significant-figure accuracy when only 20 terms are included in the series solution. That is to say, with a small number of terms in the series solution, the results by the present S-DSM show excellent accuracy when compared with the FE solutions which use a very fine mesh. Some representative mode shapes are shown in Fig. 3. It is found that Part B plays a dominant role in the first 20 mode shapes. This is to be expected since the top and bottom layers of Part A are of ply angle  $90^\circ$  which significantly stiffen the Part A structure in the direction parallel to the clamped edge. The results presented in Table 7 are probably the first set of exact solutions reported for such type of stepped cantilevered composite plate. Of course, the parametric studies with respect to the geometries and stacking sequences will be very interesting to investigate for practical significance, but this will take this paper beyond its intended purpose.

#### 4.2. A multi-span composite plate

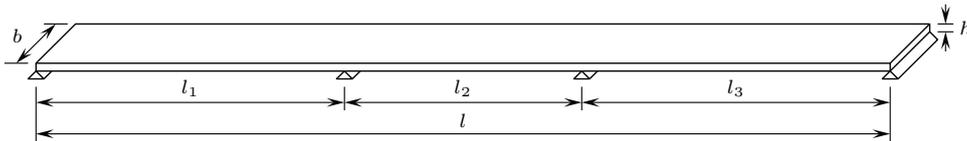


Figure 4: A three span bridge deck.

The applications of multi-span composite plates range from bridges to space platforms. The dynamic analysis of such structures can not be overemphasized. In particular, bridges decks may be idealised as continuous rectangular composite plates simply supported at its two ends and may be with some intermediate supports whereas the rest edges are free, see Fig. 4. This can be a challenging task involving multi-span plates with practical applications. There are a few analytical solutions for this case [26, 27, 28]. Zhu and Law [27] applied the Rayleigh-Ritz method using eigenfunctions of multi-span beam together with those of a single-span beam. Gorman and Garibaldi [28] used the superposition method and span-by-span approach to obtain accurate analytical solutions for multi-span *isotropic*

Table 8: The first 16 natural frequencies for a three-span orthotropic bridge deck.

Mode	Natural frequencies ( $Hz$ )				Relative Error (%)		
	S-DSM	FEM [26]	Semi-Anal.[26]	Ritz(beam) [27]	S-DSM/FEM	S-DSM/Semi-Anal.	S-DSM/Ritz(beam)
1	<b>4.1295</b>	4.13	4.13	4.13	0.01	0.01	0.01
2	<b>5.4469</b>	5.45	5.45	4.70	0.06	0.06	-13.71
3	<b>6.3019</b>	6.30	6.30	6.31	-0.03	-0.03	0.13
4	<b>7.5866</b>	7.59	7.59	6.86	0.05	0.05	-9.58
5	<b>7.7582</b>	7.76	7.75	7.76	0.02	-0.11	0.02
6	<b>8.7911</b>	8.79	8.77	8.20	-0.01	-0.24	-6.72
7	<b>8.9957</b>	9.00	9.08	missed	0.05	0.94	-
8	<b>11.228</b>	11.23	11.26	missed	0.02	0.29	-
9	<b>12.003</b>	12.01	11.97	missed	0.06	-0.28	-
10	<b>14.856</b>	14.88	15.07	missed	0.16	1.44	-
11	<b>15.800</b>	15.80	15.79	15.81	0.00	-0.07	0.06
12	<b>17.165</b>	17.17	17.16	16.39	0.03	-0.03	-4.52
13	<b>17.230</b>	17.26	17.33	missed	0.18	0.58	-
14	<b>17.696</b>	17.73	17.65	missed	0.19	-0.26	-
15	<b>21.162</b>	21.17	21.19	missed	0.04	0.13	-
16	<b>22.275</b>	22.28	22.27	22.29	0.02	-0.02	0.07

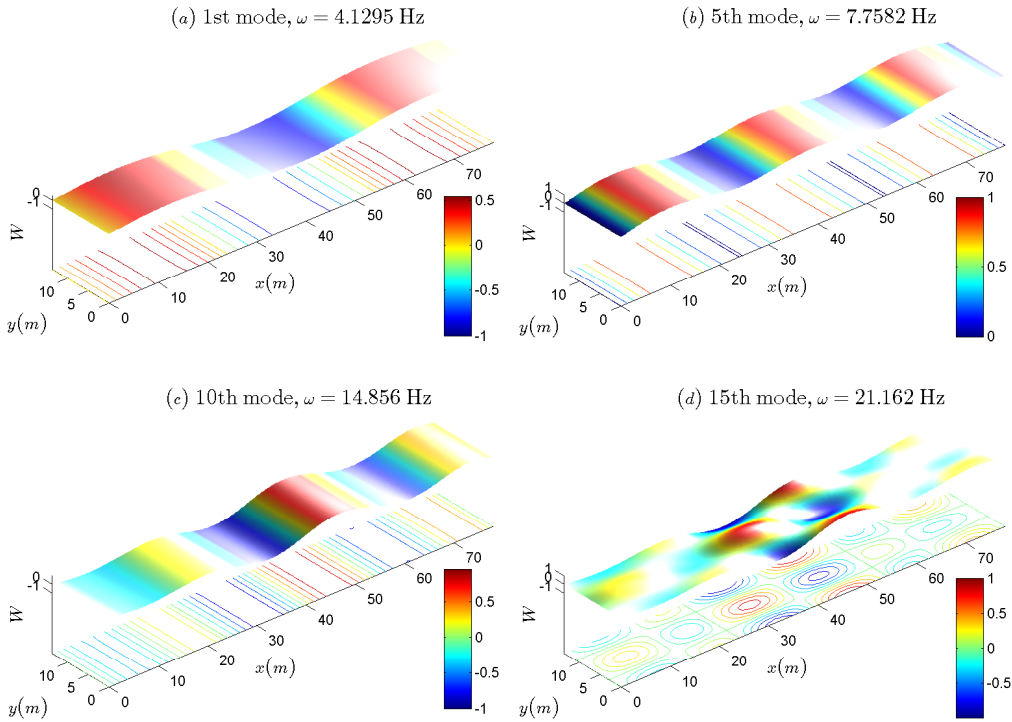


Figure 5: The 1st, 5th, 10th and 15th natural modes of a three-span composite bridge.

bridge decks. Rezaiguia and Laefer [26] proposed a semi-analytical approach for three-span orthotropic bridge deck based on modal method. Now the current S-DSM is used to revisit the problem which was discussed at some length in Refs.

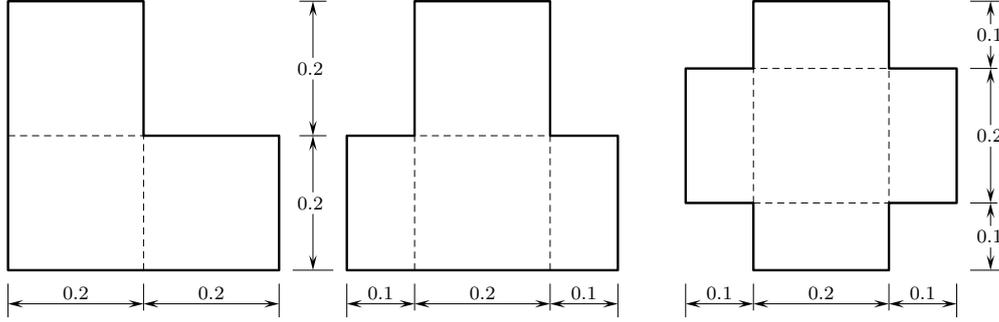


Figure 6: The geometries of L-, T- and cross- shaped plates made of T-graphite/epoxy material (length unit:  $m$ ). The dashed lines indicate the domain discretisation in the S-DSM application.

[26, 27].

It is a three-span continuous orthotropic bridge deck, as illustrated in Fig. 4. The geometry and material properties are adopted to be the same as in Refs. [26, 27]:

$$l = 78m, l_1 = l_3 = 24m, l_2 = 30m, b = 13.715m, h = 0.21157m, \rho = 3265.295kgm^{-3},$$

$$D_x = 2.4150 \times 10^9 Nm, D_y = 2.1807 \times 10^7 Nm, D_{xy} = 1.1424 \times 10^8 Nm, \nu_{xy} = 0.3.$$

The first 16 natural frequencies are computed by the S-DSM which are compared and contrasted with those from the FEM (ANSYS), the Ritz [27] and the semi-analytical [26] methods, see Table 8. In the application of the S-DSM, three plate elements are used to represent the three spans of the bridge respectively. All of the results computed by S-DSM have accuracy up to five significant figures. It is clear from Table 8 that the FEM results using ANSYS given in Ref. [26] are in better agreement with the current S-DSM results than those computed by the semi-analytical [26] and Ritz [27] methods. The results obtained by Ritz methods [27] using beam characteristic equations have the lowest accuracy. Some of the natural frequencies are even missed in the analysis using Ritz method [27]. Four representative mode shapes computed by the current S-DSM are illustrated in Fig.5.

#### 4.3. L, T and cross-shaped composite plates

Irregularly shaped plates with orthogonal straight edges such as L, T and cross-shaped plates are quite often encountered in practice. The free vibration analysis of such plates plays an important role to characterise their dynamic behaviour. However, due to the difficulties in coping with the complexity of the geometry, there were limited analytical solutions on the free vibration behaviour of these irregularly shaped plates under different boundary conditions. The problem seems to be first investigated by Irie *et al.* [29] using a series-type method but

only with all edges of the plate clamped. Liew and Sum [30] used Ritz method based on beam characteristic polynomials to solve the same problem. Solecki [31], on the other hand, studied a simply supported L-shaped plate which was treated as a rectangular plate with a cutout and he subsequently transferred the problem into a boundary integral equations. However, all of the above methods are basically limited to isotropic plates with specific boundary conditions, and the results reported in the literature are not sufficiently accurate. On the contrary, the current S-DSM provides a versatile tool to handle problems of this nature with arbitrary boundary conditions in a completely satisfactory manner. Furthermore, this method enables one to compute the results to any desired accuracy. For illustrative purposes, three different shapes of composite plates of complex geometries are taken into consideration. These are L-shaped, T-shaped and cross(+)-shaped plates. The geometries are shown in Fig. 6. Two representative sets of boundary conditions for these three cases are considered. One set for fully clamped edges and the other set is for completely free edges. The plates are made of single layer T-graphite/epoxy with thickness  $0.1mm$  and ply angle  $0^\circ$ :  $E_1 = 185GPa$ ,  $E_2 = 10.5GPa$ ,  $G_{12} = 7.3GPa$ ,  $\nu_{12} = 0.28$ ,  $\rho = 1600kg/m^3$ . The L, T and cross-shaped plates are modelled respectively using three, four and five DS plate elements in the S-DSM application. The domain discretisation is illustrated by the dashed lines in Fig 6. (Alternatively, the symmetric properties of both the T- and the cross-shaped plates can, of course, be taken advantage of to simplify further into L-shaped plates with corresponding boundary conditions.) All S-DSM results are presented with five significant digit precision, which are compared with those computed from the FEM package ABAQUS, see Table 9. As shown in Table 9, most of the FEM solutions with a very fine mesh (over 10000 el-

Table 9: First eight natural frequencies of L, T and cross-shaped plates with all of the edges clamped or free. The results computed by the current S-DSM are compared with FEM solutions with ABAQUS using a very fine mesh (over  $10^5$  elements).

B.C.	Plate shape		$\omega$ (Hz)							
			1	2	3	4	5	6	7	8
Fully clamped	L	S-DSM	<b>9.9094</b>	<b>19.168</b>	<b>21.059</b>	<b>26.598</b>	<b>28.647</b>	<b>31.115</b>	<b>34.575</b>	<b>38.693</b>
		FEM	9.8959	19.145	21.035	26.562	28.620	31.068	34.529	38.659
	T	S-DSM	<b>9.5126</b>	<b>17.791</b>	<b>21.046</b>	<b>27.703</b>	<b>28.500</b>	<b>29.473</b>	<b>33.697</b>	<b>39.046</b>
		FEM	9.5132	17.794	21.046	27.705	28.504	29.476	33.701	39.048
	+	S-DSM	<b>9.0601</b>	<b>15.956</b>	<b>20.938</b>	<b>24.979</b>	<b>27.962</b>	<b>30.202</b>	<b>33.867</b>	<b>39.022</b>
		FEM	9.0609	15.959	20.939	24.985	27.966	30.205	33.871	39.025
Completely free	L	S-DSM	<b>1.3868</b>	<b>2.1698</b>	<b>3.2964</b>	<b>4.8211</b>	<b>6.7732</b>	<b>7.7119</b>	<b>8.1094</b>	<b>9.4729</b>
		FEM	1.3870	2.1705	3.2969	4.8207	6.7739	7.7024	8.1151	9.4671
	T	S-DSM	<b>1.5275</b>	<b>2.1413</b>	<b>3.7774</b>	<b>4.4616</b>	<b>7.1329</b>	<b>8.0824</b>	<b>8.3893</b>	<b>9.4339</b>
		FEM	1.5277	2.1413	3.7775	4.4617	7.1330	8.0827	8.3899	9.4342
	+	S-DSM	<b>1.8496</b>	<b>2.4079</b>	<b>4.1540</b>	<b>5.1349</b>	<b>7.0265</b>	<b>7.1996</b>	<b>8.5729</b>	<b>9.5514</b>
		FEM	1.8497	2.4079	4.1543	5.1351	7.0272	7.1997	8.5735	9.5519

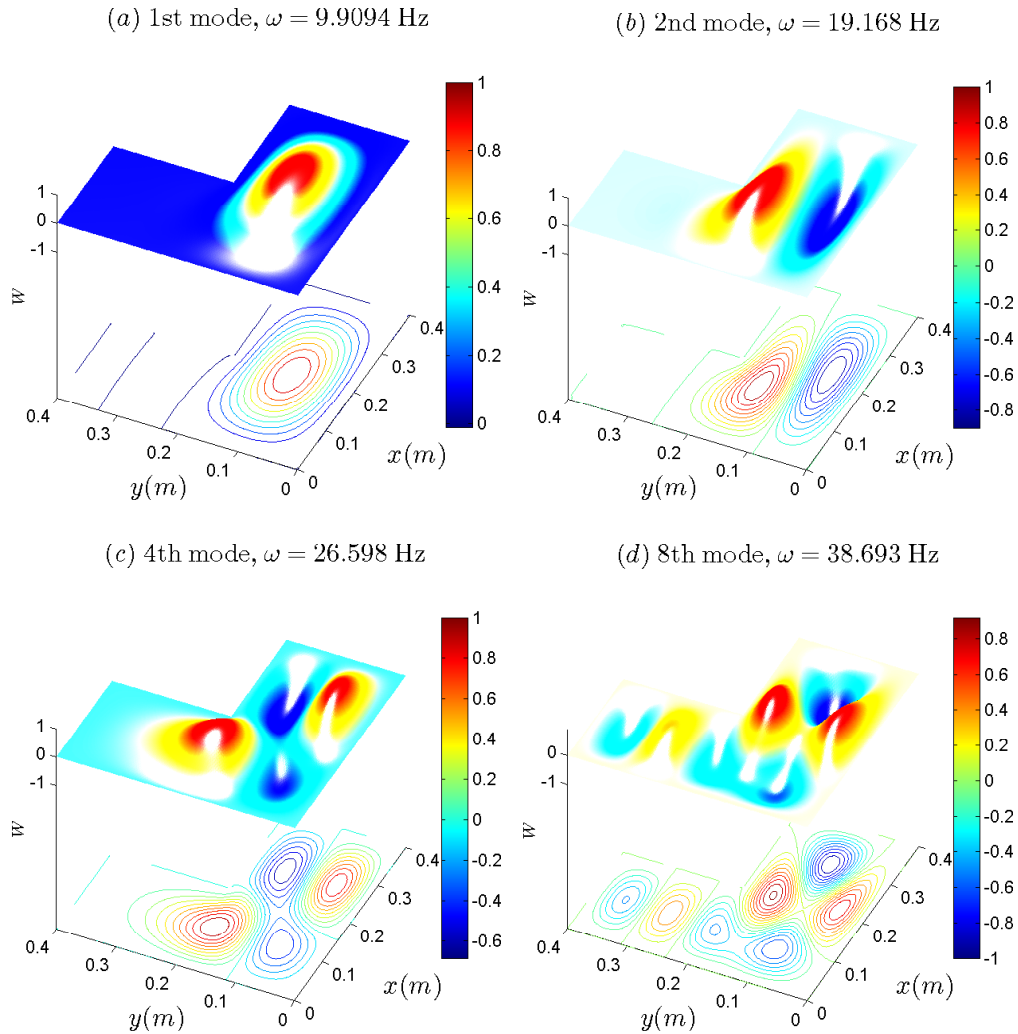


Figure 7: The 1st, 2nd, 4th and 8th natural modes of a fully clamped L-shaped T-graphite/epoxy lamina.

ements) coincide with those computed by S-DSM with four coincident digits, exhibiting very good agreement. Representative mode shapes for the fully clamped and completely free L-shaped plates are depicted in Figs. 7 and 8. Another set of representative modes in Figs. 9 and 10 are shown for clamped and completely free composite cross-shaped plates. Of course, the current S-DSM can be easily applied to more complex geometries with arbitrary boundary conditions.

## 5. Conclusions

The spectral-dynamic stiffness method (S-DSM) developed in Part I of this two-part paper has been applied to a variety of plate-like structures including in-

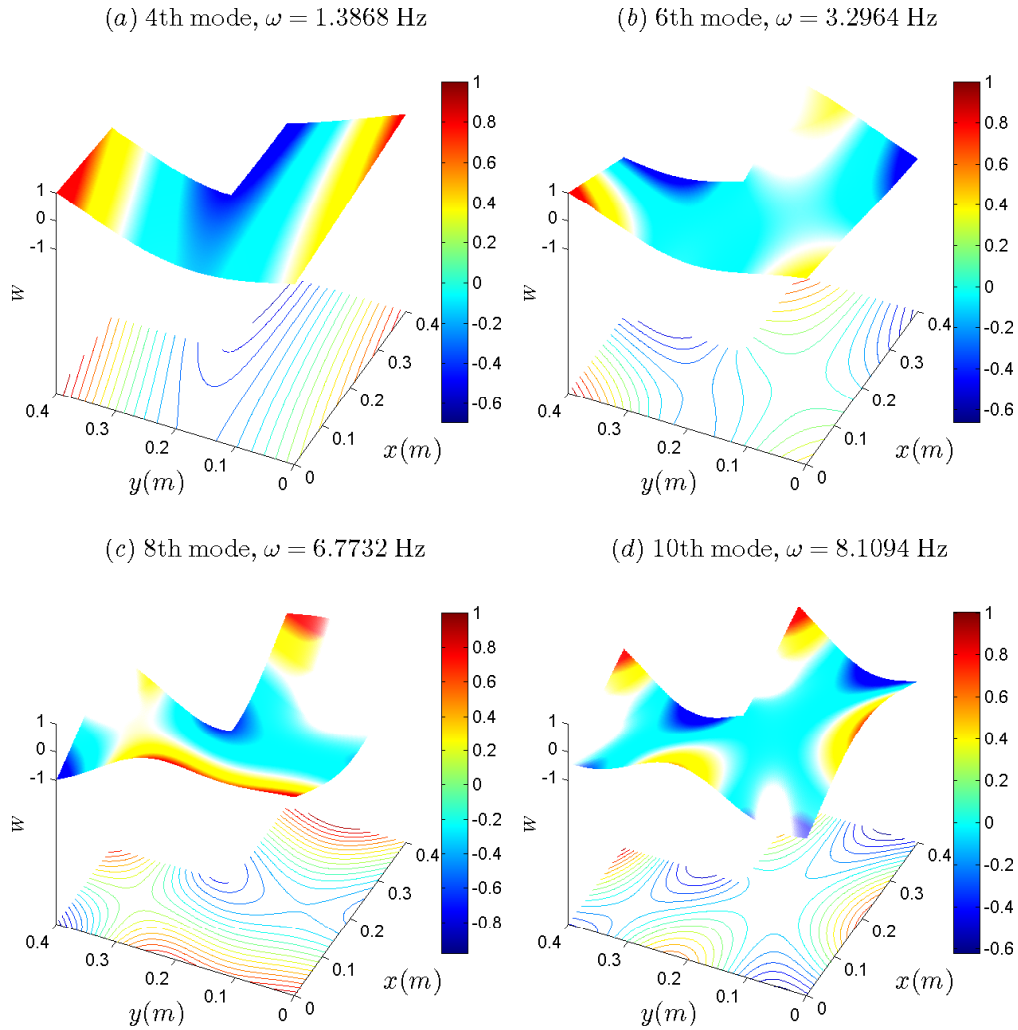


Figure 8: The 4th, 6th, 8th and 10th natural modes of a completely free L-shaped T-graphite/epoxy lamina.

dividual composite plates and complex plate assemblies with arbitrary boundary conditions. The comprehensive set of results obtained by the S-DSM are compared and contrasted with different other methods wherever possible, e.g., exact solution, finite element method, analytical methods like superposition method, Ritz method and etc. These validation exercise has been carried out to ascertain the superiority of the proposed method (S-DSM). The novelty of the S-DSM is demonstrated both in terms of accuracy as well as in terms of computational efficiency. It has been shown that the proposed S-DSM has at least a 100-fold advantage in computational time over the conventional finite element method. The exactness and high computational efficiency of the S-DSM apply to free vibration

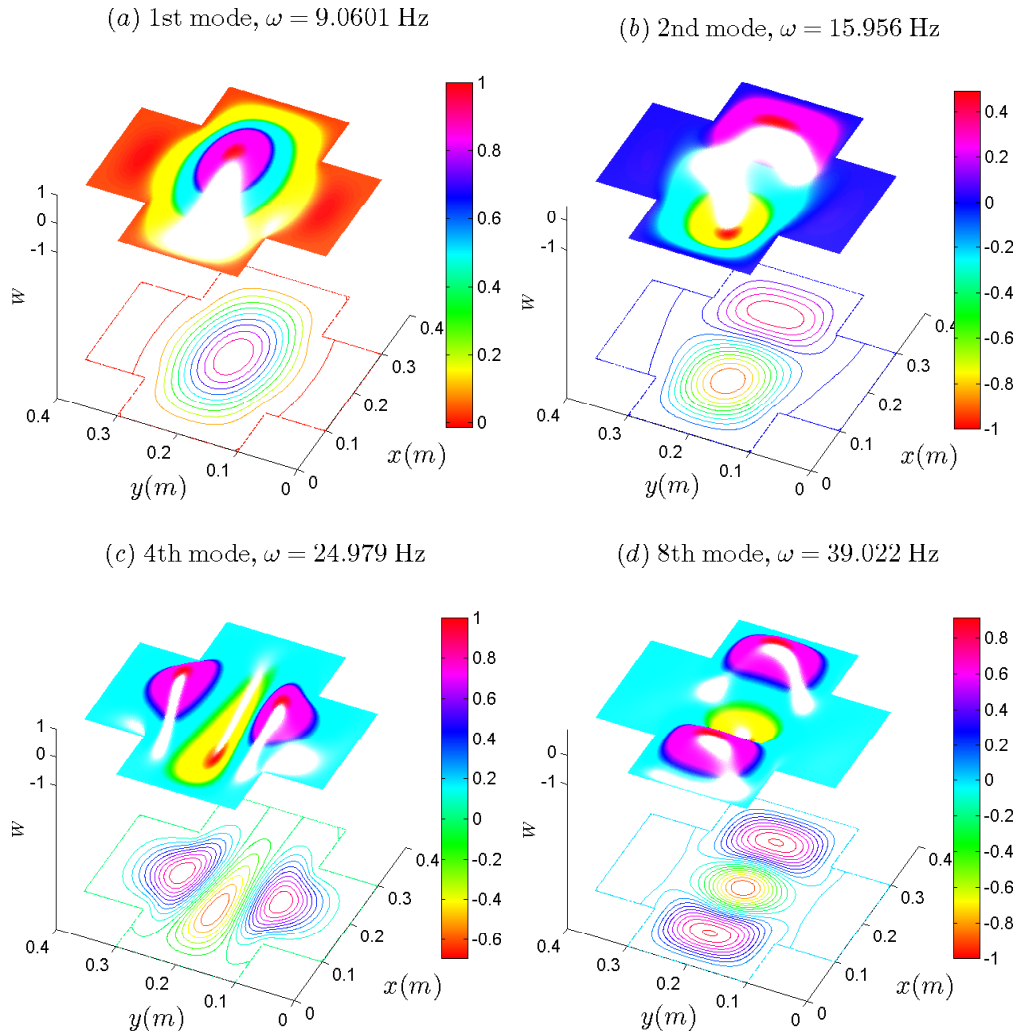


Figure 9: The 1st, 2nd, 4th and 8th natural modes of a fully clamped cross-shaped T-graphite/epoxy lamina.

analysis not only within low frequency range but also within medium to high frequency ranges. This has been assisted by the application of the enhanced Wittrick-William algorithm developed in Part I of the paper. Free vibration analysis of individual composite plates for four representative cases with different boundary conditions has been considered in detail by using the S-DSM. Besides, the computed results show good agreement with published results and also with finite element solutions. The current S-DSM is extremely versatile. It has been applied to different complex practical structures in this paper. For illustrative purposes, three examples have been considered, which are: a cantilevered laminated plate with variable thickness, a three-span continuous composite bridge deck, three irregu-

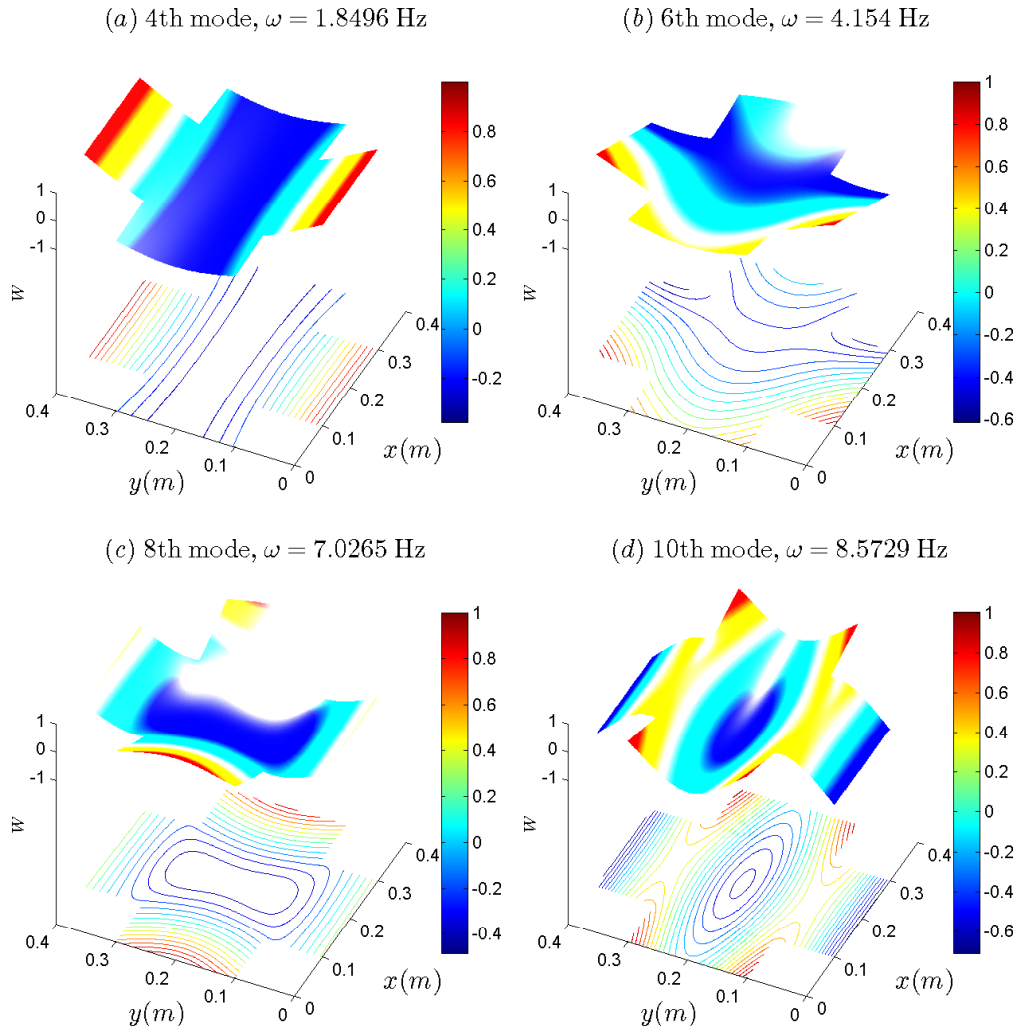


Figure 10: The 4th, 6th, 8th and 10th natural modes of a completely free cross-shaped T-graphite/epoxy lamina.

larly shaped composite plates. All of the S-DSM results presented in this paper are accurate up to all figures presented. These results may serve as benchmark solutions. It is of great significance that the development of S-DSM has provided an efficient and robust approach to carry out exact free vibration analysis of plate-like orthotropic composite structures in a very general sense.

### Acknowledgements

The authors appreciate the support given by EPSRC through a Grant EP/J007706/1 which made this work possible.

## References

- [1] X. Liu, J. R. Banerjee, An exact spectral-dynamic stiffness method for free flexural vibration analysis of orthotropic composite plate assemblies - Part I: Theory (submitted), *Composite Structures*.
- [2] X. Liu, J. R. Banerjee, Exact free vibration analysis for plates with arbitrary boundary conditions using a novel spectral-dynamic stiffness method (submitted), *Computers & Structures*.
- [3] Y. B. Zhao, G. W. Wei, Y. Xiang, Discrete singular convolution for the prediction of high frequency vibration of plates, *International Journal of Solids and Structures* 39 (2002) 65–88. doi:10.1016/S0020-7683(01)00183-4.
- [4] G. W. Wei, Y. B. Zhao, Y. Xiang, A novel approach for the analysis of high-frequency vibrations, *Journal of Sound and Vibration* 257 (2) (2002) 207–246. doi:10.1006/jsvi.5055.
- [5] L. Dozio, On the use of the Trigonometric Ritz method for general vibration analysis of rectangular Kirchhoff plates, *Thin-Walled Structures* 49 (1) (2011) 129–144. doi:10.1016/j.tws.2010.08.014.
- [6] S. Zhao, G. W. Wei, Y. Xiang, DSC analysis of free-edged beams by an iteratively matched boundary method, *Journal of Sound and Vibration* 284 (2005) 487–493. doi:10.1016/j.jsv.2004.08.037.
- [7] X. Wang, S. Xu, Free vibration analysis of beams and rectangular plates with free edges by the discrete singular convolution, *Journal of Sound and Vibration* 329 (10) (2010) 1780–1792. doi:10.1016/j.jsv.2009.12.006.
- [8] R. D. Marangoni, L. M. Cook, N. Basavanhally, Upper and lower bounds to the natural frequencies of vibration of clamped rectangular orthotropic plates, *International Journal of Solids and Structures* 14 (8) (1978) 611–623. doi:10.1016/0020-7683(78)90001-X.
- [9] R. B. Bhat, Natural frequencies of rectangular plates using characteristic orthogonal polynomials in Rayleigh-Ritz method, *Journal of Sound and Vibration* 102 (4) (1985) 493–499. doi:10.1016/S0022-460X(85)80109-7.
- [10] T. Sakata, K. Hosokawa, Vibrations of clamped orthotropic rectangular plates, *Journal of Sound and Vibration* 125 (3) (1988) 429–439. doi:10.1016/0022-460X(88)90252-0.

- [11] D. J. Gorman, Accurate free vibration analysis of clamped orthotropic plates by the method of superposition, *Journal of Sound and Vibration* 140 (3) (1990) 391–411. doi:10.1016/0022-460X(90)90758-R.
- [12] T. Sakata, K. Takahashi, R. B. Bhat, Natural frequencies of orthotropic rectangular plates obtained by iterative reduction of the partial differential equation, *Journal of Sound and Vibration* 189 (1) (1996) 89–101. doi:10.1006/jsvi.1996.9999.
- [13] Y. F. Xing, B. Liu, New exact solutions for free vibrations of thin orthotropic rectangular plates, *Composite Structures* 89 (4) (2009) 567–574. doi:10.1016/j.compstruct.2008.11.010.
- [14] A. Bahrami, M. N. Bahrami, M. R. Ilkhani, Comments on New exact solutions for free vibrations of thin orthotropic rectangular plates, *Composite Structures* 107 (2014) 745–746. doi:10.1016/j.compstruct.2013.09.064.
- [15] A. W. Leissa, The free vibration of rectangular plates, *Journal of Sound and Vibration* 31 (3) (1973) 257–293. doi:10.1016/S0022-460X(73)80371-2.
- [16] D. J. Gorman, Accurate free vibration analysis of the completely free orthotropic rectangular plate by the method of superposition, *Journal of Sound and Vibration* 165 (3) (1993) 409–420. doi:10.1006/jsvi.1993.1267.
- [17] W. L. Li, X. Zhang, J. Du, Z. Liu, An exact series solution for the transverse vibration of rectangular plates with general elastic boundary supports, *Journal of Sound and Vibration* 321 (1-2) (2009) 254–269. doi:10.1016/j.jsv.2008.09.035.
- [18] H. Khov, W. L. Li, R. F. Gibson, An accurate solution method for the static and dynamic deflections of orthotropic plates with general boundary conditions, *Composite Structures* 90 (4) (2009) 474–481. doi:10.1016/j.compstruct.2009.04.020.
- [19] A. W. Leissa, Frequencies and mode shapes of cantilevered laminated composite plates, *Journal of Sound and Vibration* 154 (1) (1992) 161–172.
- [20] J. R. Banerjee, X. Liu, H. I. Kassem, Aeroelastic stability analysis of high aspect ratio aircraft wings, *Journal of Applied Nonlinear Dynamics* 3 (4) (2014) 413–422. doi:10.5890/JAND.2014.12.012.

- [21] D. J. Gorman, R. Singhal, Free Vibration Analysis of Cantilever Plates With Step Discontinuities in Properties By the Method of Superposition, *Journal of Sound and Vibration* 253 (3) (2002) 631–652. doi:10.1006/jsvi.2001.4067.
- [22] D. J. Gorman, Free vibration analysis of cantilever plates by the method of superposition, *Journal of Sound and Vibration* 49 (4) (1976) 453–467. doi:10.1016/0022-460X(76)90828-2.
- [23] D. J. Gorman, Accurate free vibration analysis of the orthotropic cantilever plate, *Journal of Sound and Vibration* 181 (4) (1995) 605–618. doi:10.1006/jsvi.1995.0161.
- [24] J. Seok, H. F. Tiersten, H. A. Scarton, Free vibrations of rectangular cantilever plates. Part 1: out-of-plane motion, *Journal of Sound and Vibration* 271 (1-2) (2004) 131–146. doi:10.1016/S0022-460X(03)00365-1.
- [25] Y. J. Liu, G. R. Buchanan, Free vibration of stepped cantilever Mindlin plates, *Journal of Sound and Vibration* 271 (2004) 1083–1092. doi:10.1016/S0022-460X(03)00777-6.
- [26] A. Rezaiguia, D. F. Laefer, Semi-analytical determination of natural frequencies and mode shapes of multi-span bridge decks, *Journal of Sound and Vibration* 328 (3) (2009) 291–300. doi:10.1016/j.jsv.2009.08.007.
- [27] X. Q. Zhu, S. S. Law, Dynamic Load on Continuous Multi-Lane Bridge Deck From Moving Vehicles, *Journal of Sound and Vibration* 251 (4) (2002) 697–716. doi:10.1006/jsvi.2001.3996.
- [28] D. J. Gorman, L. Garibaldi, Accurate analytical type solutions for free vibration frequencies and mode shapes of multi-span bridge decks: the span-by-span approach, *Journal of Sound and Vibration* 290 (1-2) (2006) 321–336. doi:10.1016/j.jsv.2005.03.020.
- [29] T. Irie, G. Yamada, Y. Narita, Free vibration of cross-shaped, I-shaped and L-shaped plates clamped at all edges, *Journal of Sound and Vibration* 61 (4) (1978) 571–583. doi:10.1016/0022-460X(78)90456-X.
- [30] K. M. Liew, Y. K. Sum, Vibration of plates having orthogonal straight edges with clamped boundaries, *Journal of Engineering Mechanics* 124 (1998) 184–192. doi:10.1061/(ASCE)0733-9399(1998)124:2(184).

- [31] R. Solecki, Vibration of a simply supported L-shaped plate, *Journal of Vibration and Acoustics* 119 (1997) 464–467. doi:10.1115/1.2889746.